2015

The role of compaction energy on the small strain properties of a compacted silty sand subjected to drying - wetting cycles

A Heitor
University of Wollongong, aheitor@uow.edu.au

B Indraratna
University of Wollongong, indra@uow.edu.au

C Rujikiatkamjorn
University of Wollongong, cholacha@uow.edu.au

The role of compaction energy on the small strain properties of a compacted silty sand subjected to drying - wetting cycles

Abstract

The elastic properties of a soil are usually investigated to describe its engineering behaviour. The results of previous studies indicate that the effect of changes in suction on the elastic response at a small strain level of soils is significant during compaction and post-compaction periods. Limited efforts have been focused on quantifying those post-compacted responses due to the changes in suction induced by wetting and drying cycles. During their service life, most earth structures experience changes in hydraulic behaviour owing to climatic changes. These seasonal fluctuations in turn impact on the geomechanical performance of compacted soil. In this paper the aspects related to the elastic properties of compacted soils subjected to cycles of drying and wetting are described. Particular emphasis is placed on the effect of compaction energy on the hysteric behaviour (i.e. amplitude of the hysteresis loop) and its dependence on the initial stress state conditions and suction history. The results not only confirm the importance of the current suction in governing the shear and compression velocities and associated moduli, but they also suggest that subsequent drying-wetting cycles or suction history can further induce hysteretic changes, particularly along the wetting paths.

Disciplines
Engineering | Science and Technology Studies

The role of compaction energy on the small strain properties of a compacted silty sand subjected to drying–wetting cycles

A. HEITOR*, B. INDRARATNA* and C. RUJIKIATKAMJORN*

The elastic properties of a soil are usually investigated to describe its engineering behaviour. The results of previous studies indicate that the effect of changes in suction on the elastic response at a small strain level of soils is significant during compaction and post-compaction periods. Limited efforts have been focused on quantifying those post-compacted responses due to the changes in suction induced by wetting and drying cycles. During their service life, most earth structures experience changes in hydraulic behaviour owing to climatic changes. These seasonal fluctuations in turn impact on the geomechanical performance of compacted soil. In this paper the aspects related to the elastic properties of compacted soils subjected to cycles of drying and wetting are described. Particular emphasis is placed on the effect of compaction energy on the hysteric behaviour (i.e. amplitude of the hysteresis loop) and its dependence on the initial stress state conditions and suction history. The results not only confirm the importance of the current suction in governing the shear and compression velocities and associated moduli, but they also suggest that subsequent drying–wetting cycles or suction history can further induce hysteretic changes, particularly along the wetting paths.

KEYWORDS: compaction; laboratory tests; partial saturation; suction

INTRODUCTION

Compacted soils are often used as construction materials for earth structures such as retaining walls, dams, foundations, and road and railway embankments, and as such are usually placed and often remain on site under partially saturated conditions. The deformation characteristics of these earth structures under repeated loading (e.g. vibrations caused by traffic of heavy and fast-moving vehicles, heavy earthwork machinery and earthquakes) are generally governed by their elastic properties at a small strain level. These properties can be readily monitored by examining the propagation of the compression and shear waves in the soil. Under a partially saturated condition, the capillary force or suction increases the inter-particle contact forces that in turn contribute to an increase in the stiffness of the soil skeleton. The body waves (i.e. compression and shear waves) propagating through a partially saturated medium are also affected by suction and associated degree of saturation. Compression waves (P-waves) induce the motion of soil grains in the direction of wave propagation and they are mainly affected by the bulk modulus of the medium, which causes them to respond to the variation of the degree of saturation (Inci *et al.*, 2003; George *et al.*, 2009; Barrière *et al.*, 2012). In contrast, shear waves propagate perpendicularly to the direction of their motion, so shear distortion is applied. While it may be thought that shear waves are almost unaffected by the presence of water, intermediate states of saturation can cause a change in shear wave velocity due to the strengthening of the soil skeleton by capillary forces (i.e. Cho & Santamarina, 2001).

Past research studies have reported that the elastic properties at a small strain level are associated with the soil water retention characteristics (SWRC) (e.g. Cho & Santamarina,

2001; Mancuso *et al.*, 2002). Indeed, a variation of the shear and compression wave velocities (V_s and V_p, respectively) is directly related to the different ranges observed in the SWRC. In particular, inflexions on the shear wave velocity and associated shear stiffness were reported at the air entry value (AEV) and at the transition from funicular to pendular states (e.g. Cho & Santamarina, 2001). In the low suction range before AEV, the shear modulus increases linearly with suction, after which its increase is predominantly non-linear, mainly due to the distinct hydraulic regulation at the particle level (Mancuso *et al.*, 2002). Similar observations were also reported for a range of different soils by Marinho *et al.* (1996); Vinale *et al.* (2001), Inci *et al.* (2003), Sawangsuriya *et al.* (2008), Biglari *et al.* (2012) and Heitor *et al.* (2012). In addition, Mancuso *et al.* (2002) and, more recently, Heitor *et al.* (2013) also reported that the small strain shear modulus depends mainly on the soil fabric derived from compaction, that is, dry and wet of optimum water content particularly in the macroporosity range. Furthermore, this change of soil microstructure caused by variations in the compaction induced states (i.e. water content and compaction effort), often results in distinct mechanical and hydraulic behaviour (Toll & Ong, 2003; Bagherieh *et al.*, 2009; Sheng & Zhou, 2011).

The effect of hydraulic hysteresis and suction history on the small strain shear modulus of a completely decomposed tuff has recently been investigated by Ng *et al.* (2009) and Ng & Xu (2012). The most striking aspect was observing the hysteresis between the drying and wetting curves, although the size of the loop was small for those soils. The results indicated that at any given suction the shear modulus along the wetting path has a higher value than along the drying path. This is associated with the changes of degree of saturation (S_r) and the water distribution in the pore structure (menisci) (Cho & Santamarina, 2001); that is, the lower the S_r the higher the G_0. Those changes of degree of saturation are caused by the ink-bottle effect (e.g. Lourenco *et al.*, 2012) and the variation in soil structure during drying–wetting cycles (e.g. Cuisinier & Laloui, 2004). In this context, the ink-bottle effect refers to the soil-water exchange occurring within the soil pores to mimic the existence of large pores connected through smaller pores. The amplitude of the

hysteresis loop increased as the isotropic confining stresses decreased. George *et al.* (2009) and Khosravi & McCartney (2012) reported similar observations for Bonny silt, while Ng & Xu (2012) analysed the experimental data in terms of the current suction ratio (CSR) and reported that the small strain shear modulus (G_0) increased by about 20% when the CSR increased from 1 to 2.

While most research studies focused on estimating the change in the elastic properties of compacted soils in relation to V_s and G_0, limited studies concentrated on the effect of hydraulic hysteresis and additional cycles of wetting and drying using specimens prepared at different compaction energy levels. This is very important given that, during their service life, most earth structures experience changes in hydraulic behaviour and their magnitude is likely to be associated with the compaction energy level imparted during their placement. The magnitude and extent of these changes may be described by the change in the depth of moisture (H_s) that is affected by climatic fluctuations (Fig. 1). H_s may be estimated based on the Thornthwaite moisture index (TMI) (Thornthwaite, 1948; SA, 1996; Fityus & Buzzi, 2008). For instance, the TMI distribution for Australian territories gives a H_s ranging from 0·5 m in coastal continental climates to 4 m deep in arid climates of central inland and the west coast of Australia (Austroads, 2004).

This paper examines the effect of drying and wetting on the shear and compression wave velocities and corresponding moduli of a compacted silty sand. Different specimens were compacted at the reference optimum moisture content (OMC) and prepared at three different energy levels and then examined. The impact of the suction history was also studied for specimens prepared at the equivalent water content and energy level. The salient aspects in relation to the hysteresis loops, the compaction energy level, the change of CSR, and additional cycles of wetting and drying were also addressed. In addition, this study aims to investigate the role of compaction energy (i.e. increase in roller passes) in the post-compaction hydraulic behaviour of fills having a water content equivalent to that of OMC. The compaction conditions adopted here are aligned with commonly used end-product acceptance criteria (e.g. dry unit weight ratio $\gamma/\gamma_{max} > 0.95$ and water content variation $w - w_{opt} = \pm 2\%$, AS 3798 (SA, 2007)).

TESTING PROGRAMME
Materials
The soil for this study was silty sand that was used extensively as embankment fill at Penrith, Australia; it has a plasticity index of 10%, a liquid limit of 25·5% and a specific gravity of 2·7, and can thus be classified as SP-SC (Unified Soil Classification System). The particle size distribution of the soil represents 89% sand, 7% silt and 4% clay size fraction (Fig. 2). Before compaction, the sample was air dried before being mixed with the required amount of water using a masonry trowel. Any lumps were disaggregated before placing the mixture in a plastic bag and keeping it overnight under constant temperature and humidity. The compaction characteristics of the sample were established using a standard Proctor compaction test (AS 1289.5.1.1-2003 (SA, 2003)). Three different levels of compaction energy ($E_1 = 243 \, kJ/m^3$, $E_2 = 530 \, kJ/m^3$ and $E_3 = 838 \, kJ/m^3$ corresponding to 41%, 89% and 140% in relation to the standard Proctor compaction energy level, respectively) were then applied to the 50 mm diameter by 100 mm high specimens using the procedures described by Heitor *et al.* (2013). The three different compaction energy levels adopted for the 50 mm diameter mould were adjusted to match the target dry unit weights obtained for the traditional Proctor mould for energy levels of $357 \, kJ/m^3$, $596 \, kJ/m^3$ and $832 \, kJ/m^3$ following the procedure reported by Sridharan & Sivapullaiah (2005). Similar procedures have been followed in numerous past studies too, for example, Seed & Chan (1959), Reddy & Jagadish (1993) and Tang *et al.* (2011), among others. These specimen dimensions were selected so the diameter and height of the specimen would minimise the near-field effects (Leong *et al.*, 2005). To illustrate the compaction behaviour, the compaction curves obtained for all energy levels are plotted in Fig. 3. The as-compacted suction (Table 1) was
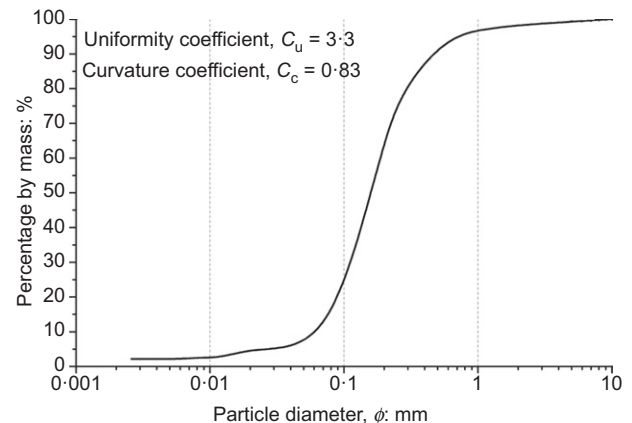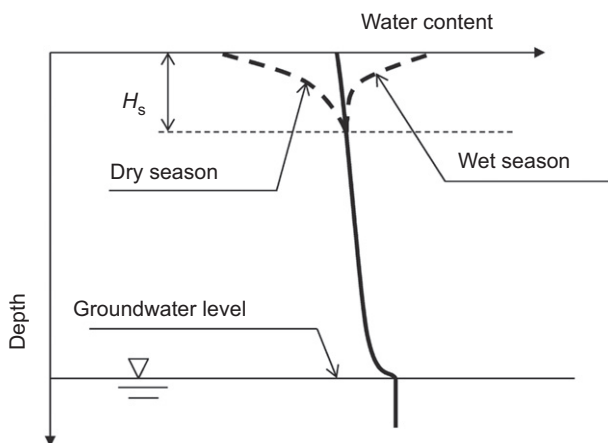

Fig. 2. Particle size distribution of silty sand

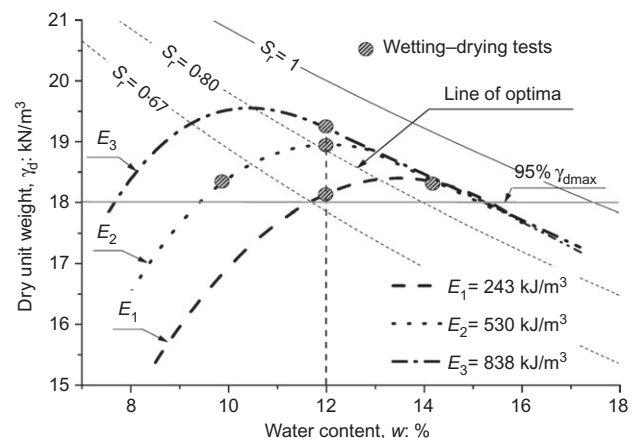Fig. 1. A profile of the groundwater content exposed to seasonal climatic variations

Fig. 3. Compaction curves for the silty sand soil illustrating the three different energy levels adopted

Table 1. Summary of the initial conditions and testing programme for the post-compacted states wetting–drying series

Test no.	Test ID	Energy level, E: kJ/m³	Water content, w: %	Dry unit weight, γ_d: kN/m³	Dry unit weight ratio, γ_d/γ_{dmax}	Tip-to-tip distance, L_{tt-i}: mm	Initial suction, $u_a - u_w$: kPa	Net confining pressure, $p - u_a$: kPa	No. of wave signals to determine, V_s, V_p
1	11-12	243	11·8	18·25	0·96	98·24	74	50	98
2	24-12	530	12·0	19·01	1	98·37	67	50	98
3	38-12	838	12·1	19·23	1·01	99·18	65	50	98
4	24-12-2	530	12·1	18·98	1	98·29	69	50	224
5	24-10	530	9·8	18·45	0·97	98·83	195	50	98
6	24-14	530	14·2	18·22	0·96	98·98	15	50	98

Note: L_{tt-i} refers to initial tip-to-tip length and suction represents the pressure differential between the top cap air pressure and bottom pedestal water pressure ($u_a - u_w$).

also routinely measured using the filter paper method (ASTM D5298 (ASTM, 2003)) and a small tip tensiometer (ASTM D3404-91 (ASTM, 2004)).

Principles of the bender–extender element test

There are two types of piezo-ceramic elements, namely *x*-poled and *y*-poled, and they differ according to their direction of polarisation; as the voltage is applied to each piezo-ceramic layer, the *x*-poled and *y*-poled elements either bend or extend if either the S-wave or P-wave is transmitted and/or received, respectively. In the bender–extender elements test a pair of piezo-ceramic elements is used; one is used as the S-wave transmitter and P-wave receiver, while the other is used as the P-wave transmitter and S-wave receiver. A schematic diagram of the bender–extender (BE) elements test set-up is shown in Fig. 4.

The small strain shear modulus G_0 can be evaluated from the shear wave velocity using the principles of elastic theory, as follows

$$G_0 = \frac{\gamma_b}{g} V_s^2 \tag{1}$$

where γ_b is the bulk unit weight (kN/m³), g is the gravity acceleration (m/s²) and V_s is the shear wave velocity (m/s). For a three-phase mixture, while assuming that the density of the air mass can be omitted (i.e. $\rho_a \cong 0$), the bulk unit weight can be calculated based on the porosity (n) and degree of saturation (S_r), as follows

$$\gamma_b = (1 - n)\gamma_w G_s + S_r n \gamma_w \tag{2}$$

Similarly, the small strain constrained modulus (M_0) can be evaluated based on the compression wave velocity (V_p) by

$$M_0 = \frac{\gamma_b}{g} V_p^2 \tag{3}$$

The elastic parameters such as small strain elastic modulus (E_0) and Poisson ratio (v) can also be defined based on the compression and shear wave velocities as follows

$$E_0 = \frac{(\gamma_b/g) V_s^2 (3V_p^2 - 4V_s^2)}{V_p^2 - V_s^2} \tag{4}$$

$$v = \frac{0·5 V_p^2 - V_s^2}{V_p^2 - V_s^2} \tag{5}$$

Shear and compression wave velocities (V_s and V_p)

To measure the V_p and V_s of the compacted specimens, a non-destructive technique using a pair of bender–extender elements (BE) was adopted in a standard triaxial apparatus. The 11 mm × 1·6 mm piezo-eletrical elements were embedded into the triaxial top cap and bottom pedestal, and protruded by 1·7 mm. A schematic diagram of the set-up is shown in Fig. 4. This system could generate and detect compression and shear waves. GDSBES v2·0 software (GDS Instruments) controlled the signal generation, while the data acquisition system had two input channels with 16-bit resolution and a sampling rate of 300–500 kHz to ensure that the resolution of the time and voltage of the input and output signals was adequate.

The BE system can potentially pick up redundant background noise from electrical sources and other sources of ambient residual vibration. The noise is random and its influence can be minimised or eliminated by sampling a larger number of signals and consistently averaging the results. The desired portion of the signal repeats systematically and its amplitude decreases in direct proportion to the number of signals that are averaged and thus the signal-to-noise ratio (SNR) is improved. This procedure is called staking and is qualitatively shown in Fig. 5. The SNR can also be enhanced by increasing the amplitude of the input signal (Leong *et al.*, 2005). It was found that a sinusoidal double amplitude wave of 10 V and systematically staking 20 sampled signals was enough to reproduce signals that were relatively free of background noise.

One of the difficulties of using bender–extender elements to measure wave velocities is selecting adequate testing variables, including the waveform and testing frequency (Leong *et al.*, 2005; Clayton, 2011). Fig. 6 shows the traces of shear and compression wave velocities obtained in a specimen compacted at 12% water content and an energy level of 529·5 kJ/m³ tested with different excitation frequencies. The time domain traces show that at excitation frequencies
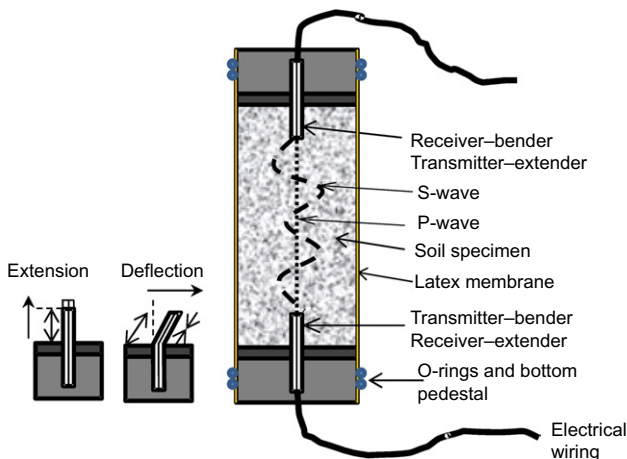
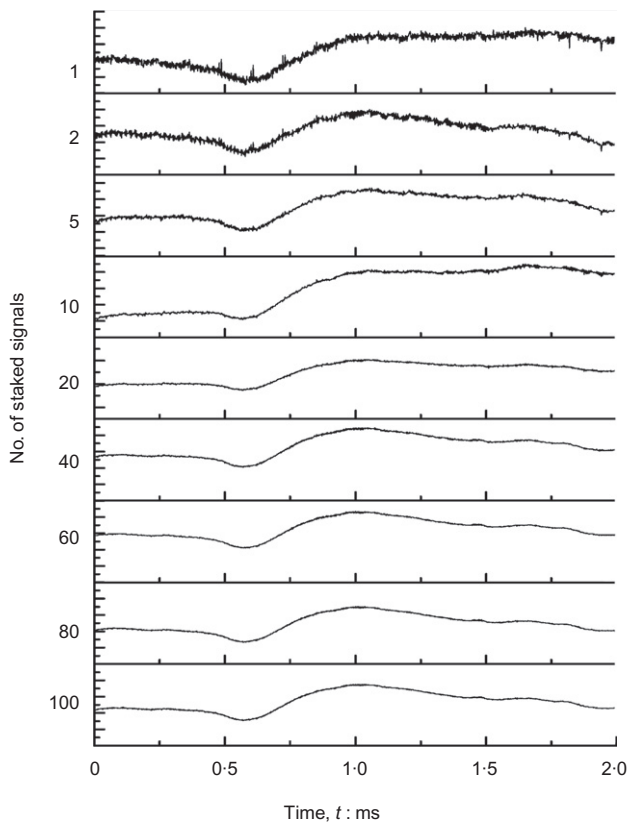Fig. 4. BE schematic illustration: principles of operation

Fig. 5. Shear wave time domain traces for increasing number of staked signals of a specimen prepared at a moisture content of 12% with compaction energy of 530 kJ/m³
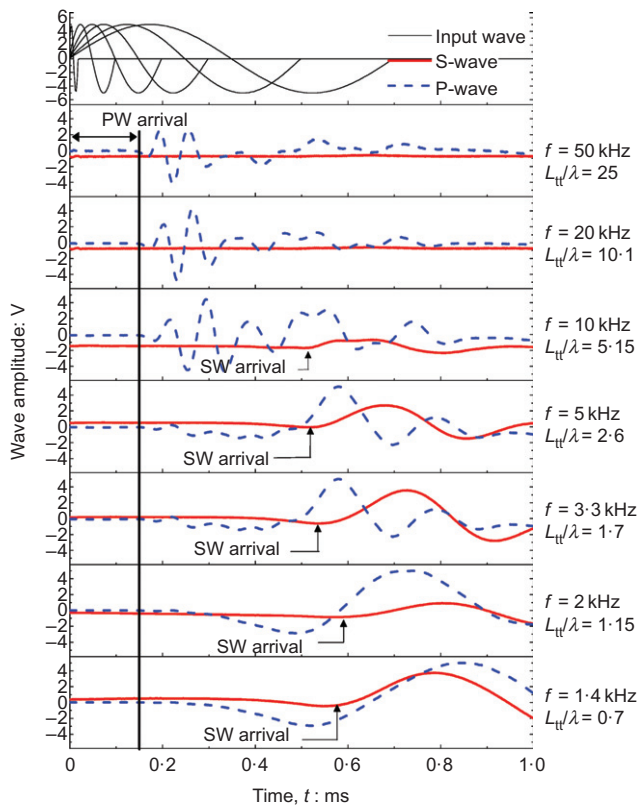

Fig. 6. Typical traces of shear (S-wave (SW)) and compression (P-wave (PW)) wave time domain for different testing frequencies varying from 1·4 to 50 kHz (specimen prepared at a compaction energy level of 530 kJ/m³ tested under unconfined conditions)

above 3·3 Hz, approximately the same travel time was observed, whereas lower values of 1·4 kHz and 2 kHz led to much larger values because of the impact of the near-field component that is associated with the propagation of other signals of opposite polarity (Sanchez-Salinero *et al.*, 1986). Thus, if only the test data collected at low testing frequencies are used to calculate V_s, then there is a danger of underestimating the shear wave velocity (V_s) obtained. The arrival of the compressional wave was determined by examining the point of first deflection in the received signal. This can either be accessed by visual inspection or using an automated procedure that detects small changes in the amplitude of the received signal for cases where visual inspection is difficult (e.g. Leong *et al.*, 2009). In this study it was found that the arrival of the compressional wave is relatively independent of the testing frequency, although the wave propagation mode seems to change for lower excitation frequencies (i.e. $f < 5$ kHz). This is possibly associated with the frequency dependence of the two kinds of waves generated during the propagation of compressional waves through solid and fluid in soil matrix (i.e. in-phase wave and out-of-phase wave). The latter tends to be highly attenuated and its effect on the results presented is relatively small.

Unlike the compression wave, the amplitude of the shear wave signal was associated with the excitation frequency, such that as the frequency increased beyond 5 kHz, the amplitude of the received signal was significantly reduced (e.g. lower than 2 V, Fig. 6). This is consistent with the findings of Arulnathan *et al.* (1998), and shows that a decrease in wavelength (λ) in relation to the bender element length ratio (l_b) contributes to the deterioration of the received signals. While it would be preferable to measure the shear wave velocity at higher testing frequencies (larger L_{tt}/λ ratios where L_{tt} is the length of the wave path), the amplitudes of received signals are often deemed unsuitable to allow for either time or frequency domain analysis. It was found that testing frequencies having a ratio between the wave path length to wavelength (L_{tt}/λ) exceeding 2 could minimise the effect of the near-field component and warrant the strength of the received signal.

The velocities of the shear and compression waves were computed based on the wave path length (L_{tt}) that corresponds to the tip-to-tip distance between the transmitter and receiver, and the travel time (Δt_s and Δt_p), as follows

$$V_s = \frac{L_{tt}}{\Delta t_s} \qquad (6)$$

$$V_p = \frac{L_{tt}}{\Delta t_p} \qquad (7)$$

The initial tip-to-tip distance was determined based on the total height of the sample, the protruding heights of the bender–extender elements and axial strain during drying–wetting cycles. The travel time of the shear wave (Δt_s) was taken as the time interval to the peak of the first bump, as described by Lee & Santamarina (2005), or to the first deflection when the first bump was not visible (Fig. 6). The travel time of the compression wave (Δt_p) was taken as the time interval to first deflection (Fig. 6).

Variation in suction during wetting and drying cycles

Suction was imposed on the specimens by applying a given air pressure by way of a top cap and a given value of water pressure beneath the high air entry value (HAEV) ceramic disc. A pressure controller accurate to 1 mm³ controlled air and water pressures applied to the specimen in a load frame

triaxial cell, while the HAEV ceramic disc had an air entry value of 15 bar. The water pressure controller had a gauge to measure the volume of water flowing into or out of the specimen as the suction changed. The criterion for equilibrium was based on the rate at which volumes of water exchanged during wetting or drying (Fig. 7), and larger volumes of water were usually exchanged along the drying paths. Fig. 7 includes selected examples of the volume of water exchange for the energy levels considered in this study (i.e. $E_1 = 247 \, \text{kJ/m}^3$, $E_2 = 530 \, \text{kJ/m}^3$ and $E_3 = 838 \, \text{kJ/m}^3$). Indeed, at E_1 the water exchange during equilibration is much larger than that of E_2 and E_3. For instance, when the specimens are dried to a suction level of 50 kPa, the volume of water exchanged is 1326 mm³, 827 mm³ and 239 mm³ for E_1, E_2 and E_3. This is mainly associated with the initial soil structure and the void ratio dependency governing the water retention behaviour (e.g. Pham et al., 2005; Tarantino & Tombolato, 2005). For larger suction levels upon drying, that is, 100 and 150 kPa, similar behaviour is observed. In contrast, when the specimens undergo wetting, the water exchange capacity is smaller and typically ranges between 434 and 609 mm³ (see Fig. 7, suction of 50 and 100 kPa). This is related to the manner in which the water intrudes the pore structure, namely ink-bottle effect (Pham et al., 2005), and this is consistent with the water retention data in Fig. 8. These data clearly demonstrate that the specimens compacted at a relatively low dry unit weight (i.e. larger voids in an aggregated structure) show a larger variation in S_r upon drying and wetting. Different levels of suction or pressure difference ($s = u_a - u_w$) were imposed on the specimens throughout the test by adjusting the water back-pressure while the air and cell pressures were kept constant (i.e. constant net confining pressure, $p - u_a$). In these tests an increment of suction in each stage was 50 kPa, while the water pressure was changed at 0·16 kPa/min and kept constant until the end of the equilibration period. Typically, a 48–60 h period was enough for the specimens to reach equilibrium. At every stage the axial displacement was also monitored within 0·001 mm, with a linear variable differential transducer (LVDT); the changes in the axial strain were small, typically within 0·01%. The drying and wetting branches of the SWRC within the range of the suction tested could be determined based on the change in the volume of water in each step. At the end of the test the water content of the specimen was determined by the oven dried method and the differences in the water content monitored by the water pressure controller were verified.
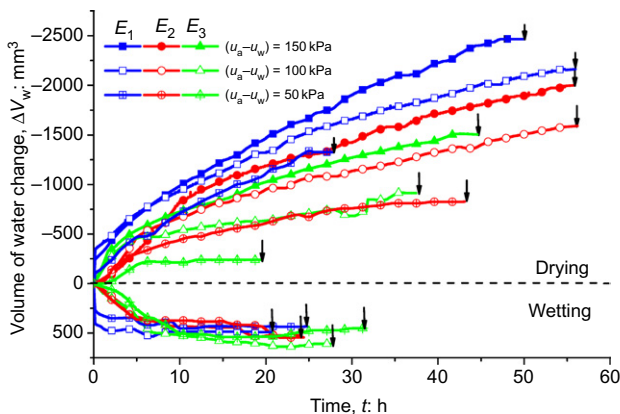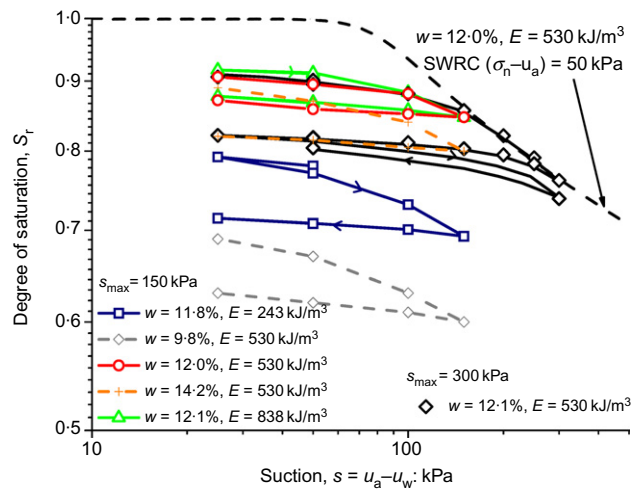

Fig. 8. Water retention data of the drying–wetting cycles of specimens prepared at different energy levels with similar water content (s_{max} = maximum suction)

Figure 8 shows the corresponding water retention data computed based on the volume of water at the end of the equilibrium stages. The SWRC of a specimen compacted at an energy level of 530 kJ/m³ is given as a reference. For most of the suction levels considered (25 to 150 kPa), most specimens lay on the scanning curves (i.e. hydraulic states enclosed by the main drying or wetting curves as explained by Tarantino & Tombolato (2005)), which is basically equivalent to expected field conditions. There was a marked hysteresis along the drying and wetting paths for all four specimens (Table 1). This difference was probably due to a heterogeneous entrapment of water in the soil pore throats (i.e. the ink bottle effect) and different contact angles during drying and wetting processes. Furthermore, the extent of the hysteric response of a specimen prepared at a lower of compaction energy level (i.e. $E = 243 \, \text{kJ/m}^3$) appeared to be larger, and then progressively decreased in those specimens prepared at higher energy levels ($E = 530 \, \text{kJ/m}^3$ and $838 \, \text{kJ/m}^3$). Thus the hysteric response depends on the initial soil structure and dry unit weight (or associated degree of saturation). Typically the term hydraulic hysteresis is used to describe the variation of degree of saturation between wetting and drying paths of the SWRC for the same suction level (e.g. Pham et al., 2005). In this study, the term small strain hysteresis is used to refer to the variation of V_s and V_p between the drying and wetting paths. The equivalent changes in suction of 25–150 kPa and 25–300 kPa resulted in variations in the water content of ±1·0% and ±1·5%, respectively.

RESULTS AND DISCUSSION

Compression and shear wave velocities and associated elastic parameters

In total, six compacted specimens were tested using bender elements under constant isotropic net confining pressure ($p - u_a$) of 50 kPa, which was adopted based on an estimation of H_s (approximately 2·5 m) for Penrith (Australia), and used for V_s and V_p evaluation. An emphasis was placed on investigating the impact of the level of compaction in the post-compacted small strain behaviour of specimens subjected to drying and wetting. Their initial compaction characteristics and testing conditions selected are given in Table 1.

Fig. 7. Example of the variation of the volume of water monitored during equalisation stages for specimens prepared at $w = 11·8\%$ and $E_1 = 243 \, \text{kJ/m}^3$, $w = 12\%$ and $E_2 = 530 \, \text{kJ/m}^3$ and $w = 12·1\%$ and $E_3 = 838 \, \text{kJ/m}^3$ (arrows indicated the equilibrium of the specimens)

The tests were conducted in a load frame based triaxial cell, where V_s and V_p were monitored using bender–extender elements that were cantilevered in the 50 mm diameter top cap and HAEV bottom pedestal. At each suction step, 14 signals with frequencies of 1·4, 2, 3, 5, 10, 20 and 50 kHz were analysed to determine the travel time and associated wave velocity. An example of the wave time domain traces during the first drying–wetting cycle tested at 10 kHz is shown in Fig. 9.

The equivalent L_{tt}/λ values monitored during the drying–wetting cycle are also given as a reference. As the suction increased on the drying path, the arrival time of both compression and shear waves decreased, which resulted in an increase in the wave velocities. This change was more noticeable in the shear wave time domain traces. On the wetting path there was only slight variation in the velocity of both waves and, although the propagation mode in the first drying path was consistent, it showed some dissimilarity in the following wetting paths.

The variations in the computed shear wave velocity (V_s) of five specimens with increasing (drying) and decreasing (wetting) suction are depicted in Figs 10(a)–10(c). The most striking aspect is that V_s exhibits hysteric response and had a larger value following the wetting path. This might not correspond to the intuitive behaviour first expected, but it can be associated with the soil-water exchange in soil pores responsible for the hysteretic response seen in the SWRC (Fig. 8). In addition, microstructural studies have reported that the soil fabric during drying is also evolving into a more constricted porosity centred at the microporosity range, although it recovers some of the macroporosity when it is subsequently wetted (Cuisinier & Laloui, 2004; Monroy et al., 2010). These results are also consistent with the small strain shear modulus studies on decomposed tuff and Bonny silt conducted by Ng & Xu (2012) and Khosravi & McCartney (2012). In addition, the hysteresis amplitude showed some differences between the five specimens (Figs 10(a)–10(c)). For instance, the specimen compacted at 243 kJ/m³ with a suction of 25 kPa, had a V_s hysteresis amplitude of about 30 m/s, but at energy 530 kJ/m³ and 838 kJ/m³, it was around 24 m/s and 16 m/s, respectively. This difference was probably related to the initial macrostructure of the specimens (e.g. Bagherieh et al., 2009; Heitor et al., 2013). Furthermore, these results seem to suggest that soil compacted under lower energy (i.e. larger percentages of macropores) has a larger V_s hysteresis amplitude in cycles of drying and wetting. For the optimum moisture content of 12% (E_2), the difference in dry densities between E_2 and E_3 is not significant, whereas the dry density of E_1 is significantly smaller. This is because the soil structure would
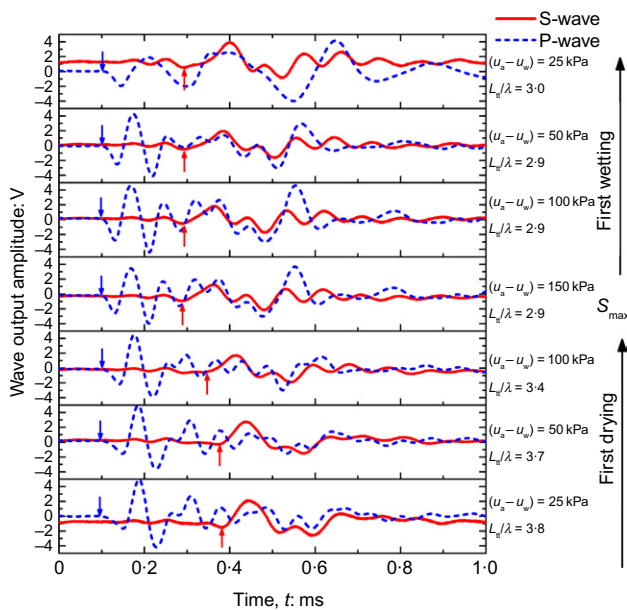

Fig. 9. Typical wave time domain traces during a drying–wetting cycle of a specimen prepared at $w = 11·8\%$ and $E = 230$ kJ/m³ for a testing frequency of 10 kHz with $L_{tt}/\lambda > 2$
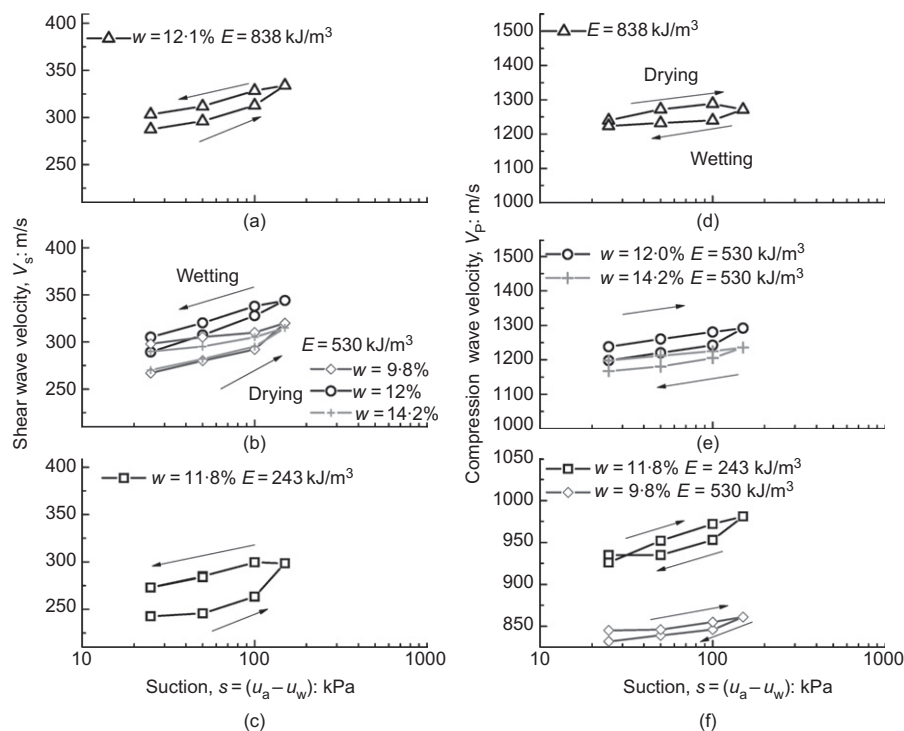

Fig. 10. Variation of V_s and V_p with suction during a drying–wetting cycle of specimens prepared at energy levels of (a) and (d) 838 kJ/m³, (b) and (e) 530 kJ/m³, and (c) and (f) 243 kJ/m³

change from an aggregated macrostructure on the dry side of OMC (i.e. $E_1 = 243$ kJ/m^3) to a progressively matrix-dominated macrostructure on the wet side of OMC (i.e. $E_3 = 838$ kJ/m^3). The role of the initial structure and associated porosity should be more influential in determining the size and shape of V_s hysteresis upon drying–wetting cycles, that is, about $V_s = 30$ m/s, 24 m/s and 16 m/s for E_1, E_2 and E_3, respectively (Fig. 10).

For E_2, the specimens compacted at 2% dry and 2% wet of OMC had similar dry unit weights, but clearly the specimen compacted on the wet side of OMC had a degree of saturation approaching 85% with a corresponding 'as-compacted' suction of 15 kPa, whereas the specimen compacted on the dry of optimum (i.e. $S_r < 65$%) sustained an 'as compacted' suction as large as 195 kPa. As illustrated in past literature through computed tomography and mercury intrusion techniques, the soil structure would also change from a predominantly aggregated assembly on the dry side of OMC to a more matrix-dominated macrostructure on the wet side of OMC (e.g. Delage et al., 1996; Monroy et al., 2010).

While the above differences in the 'as-compacted' state govern the small strain behaviour (Heitor et al., 2013), its influence is likely to become smaller when the specimens are subjected to the same suction level during drying and wetting cycles. While the specimen prepared at $w = 9.8$% might be expected to exhibit a distinctly different behaviour than that of $w = 14.2$%, the V_s values following the drying path are of similar magnitudes (Fig. 10(b)). This behaviour can be attributed to the inevitable alterations of the soil structure when specimens are brought to the same level of suction (e.g. Koliji et al., 2010). Nevertheless, the influence of the initial structure can still be observed in the V_s hysteresis loop, that is, 31 m/s for $w = 9.8$% and 20 m/s for $w = 14.2$% for suction of 25 kPa.

While the two specimens compacted on the dry side of OMC ($w = 9.8$% at E_2 and $w = 11.8$% at E_1) are likely to have a similar aggregated macrostructure (Delage et al., 1996), V_s magnitude is larger for the specimen having a higher dry unit weight, although the size of V_s hysteresis in drying and wetting is approximately the same (≈ 30 m/s). In contrast, for the two specimens compacted on the wet side of OMC ($w = 14.2$%, E_2 and $w = 12.1$%, E_3) having a matrix-dominated macrostructure, V_s magnitude is larger for the specimen having higher dry unit weight ($w = 12.1$%, E_3), whereas V_s hysteresis amplitude in drying and wetting is 20 m/s for $w = 14.2$% and 16 m/s for $w = 12.1$%. This indicates that when the specimens are brought to the same suction level, the V_s magnitude seems to be mainly dependent on their dry unit weights, whereas the V_s hysteresis seems to be influenced by the initial compacted structure. Interestingly, the specimen prepared at 243 kJ/m^3 with a corresponding maximum dry unit weight ratio of 96%, which is just borderline with respect to the common end-production specification of 95% (AS 3798 (SA, 2007)), had an hysteresis amplitude that was almost twice the one prepared at an equivalent standard Proctor energy (530 kJ/m^3). This indicates that even slight changes in compaction energy along the constant water content paths will have an important impact on the post-compacted response of compacted fills.

The variation of V_p with increasing (drying) and decreasing (wetting) suction for all three specimens is depicted in Figs 10(d)–10(f). Similarly, the compression wave velocity also exhibited hysteresis behaviour between the drying and wetting paths, but unlike V_s, the recorded V_p was higher along the drying paths. This was not surprising because the mode in which the waves propagate is different. The compressional wave propagates through both fluid and solid phases and therefore, as the degree of saturation increases or decreases, the wave velocity changes. In wetting

and drying cycles for the same suction level, the V_p variation is mainly associated with the amount of water present in the specimen; that is, the higher is the S_r value, the higher the magnitude of V_p is. In contrast, the shear wave velocity propagates only through the soil skeleton. While for fully saturated conditions it is relatively unaffected by the presence of water, under partially saturated conditions, the propagation of shear wave is more complex. Past research studies have shown that the shear wave velocity is sensitive to the degree of saturation (e.g. Cho & Santamarina, 2001); in other words, the lower is the S_r value, the higher the value of V_s is.

Figures 10(d)–10(f) also illustrates how the initial compaction history affects the V_p hysteresis characteristics. Here the hysteresis amplitude of V_p was relatively independent of the initial compaction energy level, with amplitudes ranging from 46 to 52 m/s for 230 and 838 kJ/m^3, respectively.

To simulate a different suction history, Fig. 11 shows the V_s and V_p results of an additional specimen prepared at an equivalent standard compaction energy level which was subjected higher suction (up to 300 kPa). Similarly with Fig. 10, both V_s and V_p showed a hysteretic response on the wetting paths, but while the V_s and V_p values recovered when the soil was subjected to a second cycle of drying at 300 kPa, in the subsequent wetting cycle both V_s and V_p again displayed hysteretic behaviour. The shear wave velocity showed an increase of 17 m/s, whereas the compressional wave velocity increased 30 m/s. Both V_s and V_p would be expected to show slight hysteresis on both paths, similar
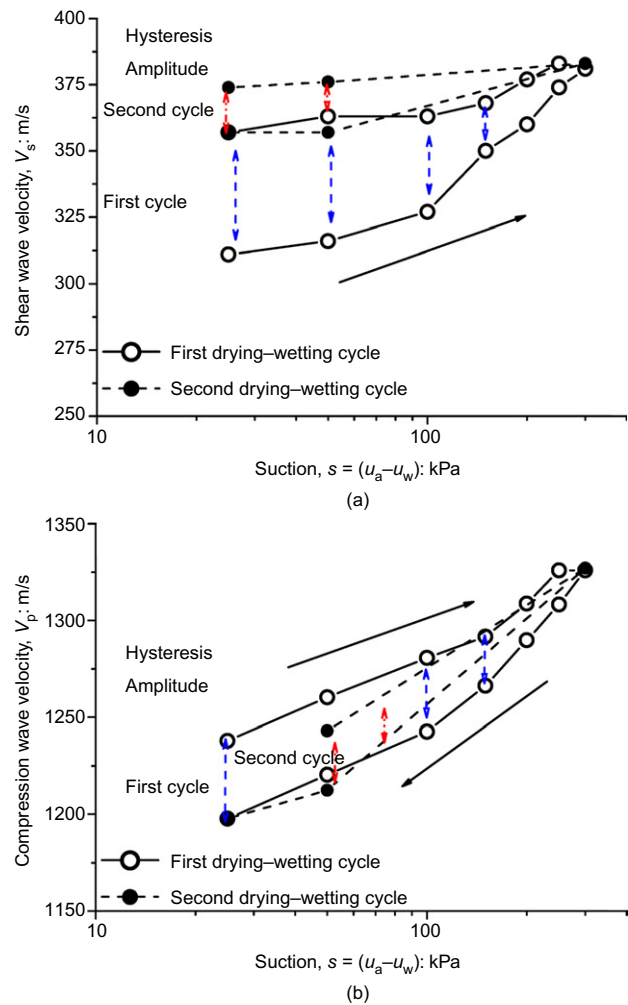

Fig. 11. Variation of (a) V_s and (b) V_p with suction for multiple drying–wetting paths of a specimen prepared at energy level 530 kJ/m^3

to the SWRC response (Fig. 8), but this was not the case. This was possibly due to changes in the soil structure. Koliji *et al.* (2010) reported that in the high suction range the volume of aggregations are reversible, whereas at low suction upon following the wetting paths it showed fewer distinguishable aggregations. Aggregations refer to the nature of the compacted soil macrostructure. Typically, compacted soil exhibits an aggregation-dominated macrostructure on the dry side and matrix-dominated on the wet side of the OMC (e.g. Delage *et al.*, 1996; Romero & Simms, 2008). Furthermore, the small strain hysteresis amplitude progressively decreases for an increasing number of drying and wetting cycles, which probably indicates that the soil experiences irrecoverable structural changes and the pore size distribution gradually becomes more uniform (i.e. Pham *et al.*, 2005). Interestingly, V_p was the same for 300 kPa level of suction, despite having a lower degree of saturation in the second cycle. This shows that in this cycle the stiffness of the soil skeleton may govern the propagation of both V_s and V_p. Furthermore, not only are the current suction and degree of saturation important, the suction history as represented by the number of drying and wetting cycles also affected the elastic response of the compacted materials.

The variation of Poisson ratio (v) computed using equation (5) is shown in Fig. 12. While for the energy levels of 530 and 838 kJ/m^3 the Poisson ratio seemed to be approximately constant during drying–wetting processes, there were some differences for the specimen compacted at a lower energy level (i.e. $E = 243$ kJ/m^3) and for the specimen prepared at water content of 9·8%. These observations are consistent with the earlier interpretation of a progressive change in the soil structure that probably occurred during the drying–wetting processes. Furthermore, while Poisson ratio still showed small variations in the first drying–wetting cycle for an energy level of 530 kJ/m^3, it remained relatively unchanged for the second drying and wetting cycle.

Shear, constrained and elastic moduli at small strain level

In Figs 13(a)–13(c), the shear modulus (G_0), constrained modulus (M_0) and elastic modulus (E_0) at a small strain level were plotted against the current suction ratio (CSR). Ng & Xu (2012) reported that the mechanical response, particularly the small strain shear modulus, can be affected by CSR, which can be defined as

$$CSR = \frac{s_{max}}{s_{current}} \tag{8}$$
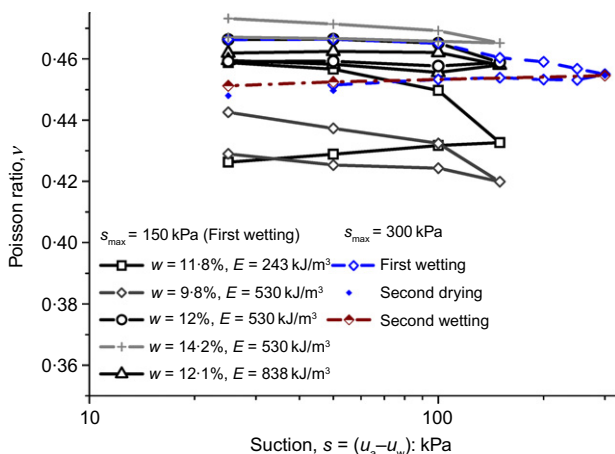

Fig. 12. Variation of the Poisson ratio with suction during drying–wetting cycles of specimens prepared at energy levels of 243 kJ/m^3, 530 kJ/m^3 and 838 kJ/m^3

where s_{max} is the maximum suction the specimen has been exposed to and $s_{current}$ is the current suction level. As expected, the specimens compacted with a higher energy level yield larger G_0, M_0 and E_0 at any given CSR, although there were noticeable differences in M_0 among the different energy levels. This was likely related to the amount of water, as reflected by the degree of saturation, of the specimens following the wetting paths, that is $S_r = 0·7$–0·72 (Fig. 8) for the energy of 243 kJ/m^3 and $S_r = 0·85$–0·88 (Fig. 8) for energy levels of 530 and 838·4 kJ/m^3, respectively. The first drying–wetting cycle of the CSR values for the drying paths were not shown because the CSR was constant and equal to unity along the drying paths. The specimen subjected to a larger variation of suction ($s_{max} = 300$ kPa) and multiple drying–wetting cycles is also included for comparison. As expected for a given CSR, the elastic moduli (G_0, M_0 and E_0) for the specimen subjected to a larger interval of suction ($s_{max} = 300$ kPa) are higher than those obtained from the specimen subjected to a suction of 150 kPa. This is because the current suction was higher (i.e. for CSR $= 3$, the current suction was 150 kPa and 50 kPa for the specimens subjected to a maximum suction of 300 and 150 kPa, respectively). Nonetheless, even with the same current suction (i.e. 25 kPa) the specimens' moduli increased significantly for a higher CSR. Furthermore, even for the same CSR, the elastic moduli seem to be affected by the number of cycles of wetting–drying. For instance, at a suction of 25 kPa (CSR $= 12$), the G_0, M_0 and E_0 differed by 25·4 MPa, 0·95 GPa and 5 MPa, respectively, between the first and second cycle. Interestingly, for the same CSR the M_0 for the specimen subjected to a larger suction interval ($s_{max} = 300$ kPa) was higher despite having a lower degree of saturation (i.e. $S_r = 0·78$–0·82, Fig. 8). This further emphasises the role of suction history on the elastic response of the compacted specimens.

To better illustrate the suction stress history at different CSRs on G_0, M_0 and E_0, the data normalised by the current stress state (p^*) were replotted in Figs 13(d)–13(f). The current stress state (p^*) can be represented by a function of the isotropic net confining pressure ($p - u_a$), suction ($u_a - u_w$) and degree of saturation (S_r), as follows

$$p^* = [(p - u_a) + (u_a - u_w)S_r] \tag{9}$$

The current stress (equation (9)) for the different compacted specimens and suction levels is given also in Table 2. The advantage of using the above relationship is that the current suction and degree of saturation (also known as effective suction), as well as the current net confining stress, are adequately accounted for in the moduli response. The justification for the inclusion of the degree of saturation in the expression of the stress state lies with the observations of the variation of V_s in wetting and drying cycles. For a given suction level, the V_s changes upon drying and wetting. This means that if the stress state is defined solely on the basis of net stress and matric suction, the observed V_s or G_0 behaviour cannot be captured. In addition, the current stress state represented in this manner is consistent with the Bishop type effective stress description widely used for partially saturated soils (e.g. Bishop, 1959; Mancuso *et al.*, 2002; Tarantino & El Mountassir, 2013).

In fact, Figs 13(d)–13(f) show that the normalised elastic moduli increased with the CSR. Furthermore, it seems that a logarithm relationship can represent the variation of the normalised moduli with CSR and different energy levels define a unique line with the exception of the specimen prepared at water content of 14·2% ($E = 530$ kJ/m^3). This implies that the elastic response was relatively independent of the compaction energy level ($s_{max} = 150$ kPa) in the normalised moduli–CSR plane, which is of great practical
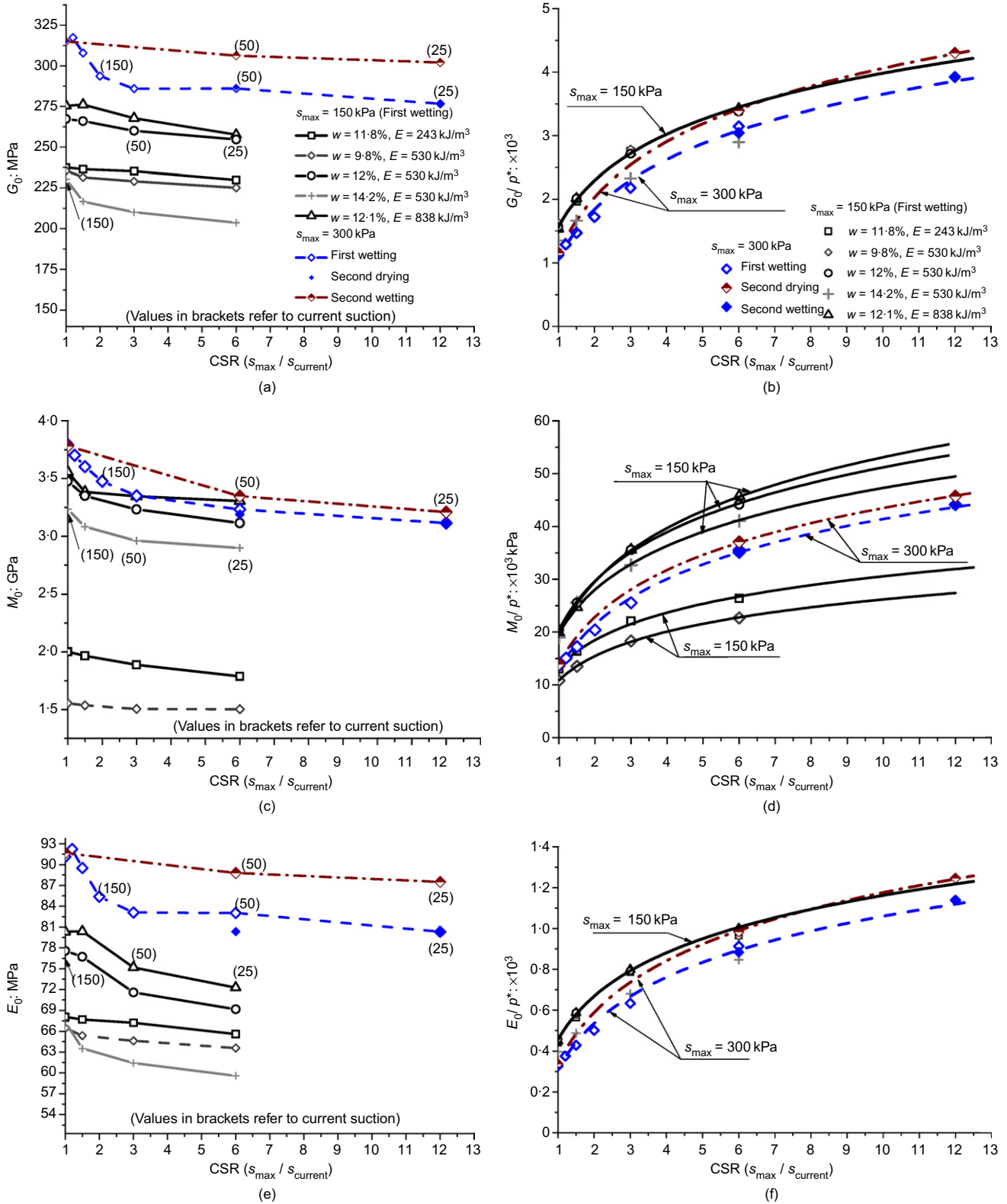
Fig. 13. Variation of G_0, M_0 and E_0 with current suction ratio (CSR) for the wetting paths of specimens prepared at energy levels of 243 kJ/m³, 530 kJ/m³ and 838 kJ/m³

significance during the time of placement because the prescribed energy level is often not defined in common end-product specifications (AS 3798 (SA, 2007)). These results suggest that $G_0/p*$ and $E_0/p*$ may be predicted for any energy level following constant water content paths provided the suction history is similar The only exception is the variation of $M_0/p*$ (Fig. 13(e)), which showed some differences between the three different energy levels, possibly

related to the large dependence of the bulk modulus of the material.

For the same CSR, the $G_0/p*$, $M_0/p*$ and $E_0/p*$ values in the first wetting of the specimen that experienced a maximum suction of 300 kPa were consistently lower than those subjected to a maximum suction of 150 kPa. However, the values of $G_0/p*$, $M_0/p*$ and $E_0/p*$ increased in the subsequent number of cycles, which indicates that the soil skeleton was

Table 2. Current stress for different suction levels (drying–wetting cycle)

Suction level: kPa	p^*: kPa				
	11–12	24–12	38–12	24–10	24–14
25	69·8	72·6	73·2	67·25	72·25
50	88·5	94·8	96·27	83·5	93·5
100	123·1	138·1	139·6	113	134
150	153·9	178·5	178·9	138·5	170
100	120·1	136·5	137·1	110	130·5
50	85·4	93·3	94·1	80·5	90·75
25	67·8	71·8	72·25	65·5	70·5

Note: p^* refers to the current stress expressed in equation (9).

strengthened with the number of drying and wetting cycles, which may be attributed to the effect of suction history and some form of hydraulic ageing.

CONCLUSIONS

From a number of bender–extender element tests conducted in specimens compacted at three different energy levels and then subjected to a post-compaction cycle of drying and wetting, the effect of variations in suction on small strain stiffness was significant. Larger values of V_s and associated G_0 corresponded to the wetting paths, a difference that was associated with the water retention properties. Furthermore, the response of V_p and M_0 depended mainly on the bulk modulus or the volume of water present because they both had lower values on the wetting paths. The initial dry unit weight and associated soil structure that resulted from preparing the specimens at different energy levels had a strong influence on the amplitude of the hysteretic response observed in a drying–wetting cycle, particularly for the V_s and associated G_0 behaviour. Larger hysteresis amplitudes were observed for specimens compacted at lower energy levels, which indicated that poorly compacted conditions can influence the post-compacted mechanical response. The suction history defined by the CSR appeared to control the elastic moduli (G_0, M_0 and E_0) to some extent but the energy level contributed to an increase in the moduli for the same CSR. However, these differences are mainly related to the current stress state because a common relationship between normalised G_0/p^* and E_0/p^*, and CSR can be obtained for different energy levels. The suction history path had a significant effect on the small strain responses, particularly for subsequent drying and wetting cycles. Finally, this study shows that the geomechanical behaviour of earth structures can be affected when exposed to changes in hydraulic regimes. This should be considered when evaluating long-term performance, particularly where fills are inadequately compacted.

ACKNOWLEDGEMENTS

NOTATION

E	compaction energy level
E_0	small strain elastic modulus
f	frequency
G_0	small strain shear modulus
g	gravity acceleration
H_s	depth of moisture change
L_{tt}	tip-to-tip distance
L_{tt-i}	initial tip-to-tip distance or wave path length
l_b	bender elements cantilevered length
M_0	small strain constrained modulus
n	porosity
p^*	current stress state
$p - u_a$	net confining pressure
S_r	degree of saturation
s	suction, or also represented by $(u_a - u_w)$
$s_{current}$	current suction
s_{max}	maximum suction the specimen has been exposed to
t	time
u_a	pore air pressure
u_w	pore water pressure
V_p	compression wave velocity
V_s	shear wave velocity
w	water content
γ_b	bulk unit weight
γ_d	dry unit weight
γ_w	water unit weight
Δt_s	shear wave travel time
Δt_p	compression wave travel time
ΔV_w	volume of water change
λ	wave length
v	Poisson ratio
ρ_a	density of the gas (air)

REFERENCES

Arulnathan, R., Boulanger, R. W. & Riemer, M. F. (1998). Analysis of bender element tests. *Geotech. Testing J.* **21**, No. 2, 120–131.

ASTM (2003). D 5298: Standard test method for measurement of soil potential (suction) using filter paper method. West Conshohocken, PA, USA: ASTM International.

ASTM (2004). D 3404-91: Standard guide for measuring matric potential in the vadose zone using tensiometers. West Conshohocken, PA, USA: ASTM International.

Austroads (2004). *Impact of climate change on road infrastructure*, AP-R243. Sydney, Australia: Ausroads.

Bagherieh, A. R., Khalili, N., Habibagahi, G. & Ghahramani, A. (2009). Drying response and effective stress in a double porosity aggregated soil. *Engng Geol.* **105**, No. 1, 44–50.

Barrière, J., Bordes, C., Brito, D., Sénéchal, P. & Perroud, H. (2012). Laboratory monitoring of P waves in partially saturated sand. *Geophys. J. Int.* **191**, No. 3, 1152–1170.

Biglari, M., d'Onofrio, A., Mancuso, C., Jafari, M. K., Shafiee, A. & Ashayeri, I. (2012). Small-strain stiffness of Zenoz kaolin in unsaturated conditions. *Can. Geotech. J.* **49**, No. 3, 311–322.

Bishop, A. W. (1959). The principle of effective stress. *Teknisk Ukeblad* **106**, No. 39, 859–863.

Cho, G. C. & Santamarina, J. C. (2001). Unsaturated particulate materials – particle level studies. *J. Geotech. Geoenviron. Engng* **127**, No. 1, 84–96.

Clayton, C. R. I. (2011). Stiffness at small strain: research and practice. *Géotechnique* **61**, No. 1, 5–37, http://dx.doi.org/10.1680/geot.2011.61.1.5.

Cuisinier, O. & Laloui, L. (2004). Fabric evolution during hydromechanical loading of a compacted silt. *Int. J. Numer. Analyt. Methods Geomech.* **28**, No. 6, 483–499.

Delage, P., Audiguier, M., Cui, Y. J. & Howat, M. D. (1996). Microstructure of a compacted silt. *Can. Geotech. J.* **33**, No. 1, 150–158.

Fityus, S. & Buzzi, O. (2008). On the use of the Thornwaite moisture index to infer depths of seasonal moisture change. *Aust. Geomech.* **43**, No. 4, 69–76.

George, L. A., Dewoolkar, M. M. & Znidarcic, D. (2009). Simultaneous laboratory measurement of acoustic and hydraulic properties of unsaturated soils. *Vadose Zone J.* **8**, No. 3, 633–642.

Heitor, A., Indraratna, B. & Rujikiatkamjorn, C. (2012). Characterising compacted soil using shear wave velocity and matric suction. *Aust. Geomech. J.* **47**, No. 2, 79–86.

Heitor, A., Indraratna, B. & Rujikiatkamjorn, C. (2013). Laboratory study of small-strain behavior of a compacted silty sand. *Can. Geotech. J.* **50**, No. 2, 179–188.

Inci, G., Yesiller, N. & Kagawa, T. (2003). Experimental investigation of dynamic response of compacted clayey soils. *Geotech. Testing J.* **26**, No. 2, 125–141.

Khosravi, A. & McCartney, J. S. (2012). Impact of hydraulic hysteresis on the small-strain shear modulus of low plasticity soils. *J. Geotech. Geoenviron. Engng* **138**, No. 11, 1326–1333.

Koliji, A., Vulliet, L. & Laloui, L. (2010). Structural characterization of unsaturated aggregated soil. *Can. Geotech. J.* **47**, No. 3, 297–297.

Lee, J. S. & Santamarina, J. C. (2005). Bender elements: performance and signal interpretation. *J. Geotech. Geoenviron. Engng* **131**, No. 9, 1063–1070.

Leong, E. C., Yeo, S. H. & Rahardjo, H. (2005). Measuring shear wave velocity using bender elements. *Geotech. Testing J.* **28**, No. 5, 1–11.

Leong, E. C., Cahyadi, J. & Rahardjo, H. (2009). Measuring shear and compression wave velocities of soil using bender-extender elements. *Can. Geotech. J.* **46**, No. 7, 792–812.

Lourenco, S. D. N., Gallipoli, D., Augarde, C. E., Toll, D. G., Fisher, P. C. & Congreve, A. (2012). Formation and evolution of water menisci in unsaturated granular media. *Géotechnique* **62**, No. 3, 193–199, http://dx.doi.org/10.1680/geot.11.P.034.

Mancuso, C., Vassallo, R. & d'Onofrio, A. (2002). Small strain behaviour of a silty sand in controlled suction resonant column-torsional shear tests. *Can. Geotech. J.* **39**, No. 1, 22–32.

Marinho, F. A. M., Chandler, R. J. & Crilly, M. S. (1996). Stiffness measurements on an unsaturated high plasticity clay using bender elements. *Proceedings of the 1st international conference on unsaturated soils*, Paris, France, vol. 1, pp. 1179–1200.

Monroy, R., Zdravkovic, L. & Ridley, A. (2010). Evolution of microstructure in compacted London Clay during wetting and loading. *Géotechnique* **60**, No. 2, 105–119, http://dx.doi.org/10.1680/geot.8.P.125.

Ng, C. W. W. & Xu, J. (2012). Effects of current suction ratio and recent suction history on small-strain behaviour of an unsaturated soil. *Can. Geotech. J.* **49**, No. 2, 226–243.

Ng, C. W. W., Xu, J. & Yung, S. Y. (2009). Effects of wetting-drying and stress ratio on anisotropic stiffness of an unsaturated soil at very small strains. *Can. Geotech. J.* **46**, No. 9, 1062–1076.

Pham, H. Q., Fredlund, D. G. & Barbour, S. L. (2005). A study of hysteresis models for soil-water characteristic curves. *Can. Geotech. J.* **42**, No. 6, 1548–1568.

Reddy, B. V. & Jagadish, K. S. (1993). The static compaction of soils. *Géotechnique* **43**, No. 2, 337–341, http://dx.doi.org/10.1680/geot.1993.43.2.337.

Romero, E. & Simms, P. (2008). Microstructure investigation in unsaturated soils: a review with special attention to contribution of mercury intrusion porosimetry and environmental scanning electron microscopy. *Geotech. Geol. Engng* **26**, No. 6, 705–722.

SA (Standards Australia) (1996). AS 2870-1996: Residential slabs and footings – construction. Sydney, Australia: Standards Australia.

SA (2003). AS 1289.5.1.1-2003: Method for testing soils for engineering purposes – soil compaction and density tests – determination of the dry density/moisture content relation of a soil using standard compactive effort. Sydney, Australia: Standards Australia.

SA (2007). AS 3798: Guidelines on earthworks for commercial and residential developments. Sydney, Australia: Standards Australia.

Sanchez-Salinero, I., Roesset, J. M. & Stokoe, K. H. (1986). *Analytical studies of body wave propagation and attenuation*, GR-85-15. Austin, TX, USA: University of Texas.

Sawangsuriya, A., Edil, T. B. & Bosscher, P. J. (2008). Modulus-suction-moisture relationship for compacted soils. *Can. Geotech. J.* **45**, No. 7, 973–983.

Seed, B. & Chan, C. K. (1959). Compacted clays: structure and strength characteristics. *J. Soil Mech. Found. Div. Trans.* **126**, No. I, 1344.

Sheng, D. & Zhou, A. N. (2011). Coupling hydraulic with mechanical models for unsaturated soils. *Can. Geotech. J.* **48**, No. 5, 826–840.

Sridharan, A. & Sivapullaiah, P. V. (2005). Mini compaction test apparatus for fine grained soils. *Geotech. Testing J.* **28**, No. 3, 1–6.

Tang, A. M., Vu, M. N. & Cui, Y. J. (2011). Effects of the maximum soil aggregates size and cyclic wetting-drying on the stiffness of a lime-treated clayey soil. *Géotechnique* **61**, No. 5, 421–429, http://dx.doi.org/10.1680/geot.SIP11.005.

Tarantino, A. & El Mountassir, G. (2013). Making unsaturated soil mechanics accessible for engineers: preliminary hydraulic-mechanical characterisation and stability assessment. *Engng Geol.* **165**: 89–104.

Tarantino, A. & Tombolato, S. (2005). Coupling of hydraulic and mechanical behaviour in unsaturated compacted clay. *Géotechnique* **55**, No. 4, 307–317, http://dx.doi.org/10.1680/geot.2005.55.4.307.

Thornthwaite, C. W. (1948). An approach toward a rational classification of climate. *Soil Sci.* **66**, No. 1, 77.

Toll, D. G. & Ong, B. H. (2003). Critical-state parameters for an unsaturated residual sandy clay. *Géotechnique* **53**, No. 1, 93–103, http://dx.doi.org/10.1680/geot.2003.53.1.93.

Vinale, F., D'Onofrio, A., Mancuso, C., Santucci de Magistris, F. & Tatsuoka, F. (2001). The pre-failure behaviour of soils as construction materials. *Proceedings of the 2nd international conference on prefailure deformation characteristics of geomaterials*, Torino, Italy, vol. 2, pp. 955–1007.